Received 23 June 2023; revised 8 August 2023; accepted 17 August 2023. Date of publication 28 August 2023; date of current version 18 September 2023.

Digital Object Identifier 10.1109/OJAP.2023.3309297

A Dual-Band Dual-Polarized Base Station Antenna Array With Isolation Enhancement

LEI GE (Senior Member, IEEE), YINHUI WANG, MINGYE DU, WEIYANG LIU, AND YUE ZHAO

State Key Laboratory of Radio Frequency Heterogeneous Integration, Shenzhen University, Shenzhen 518060, China

CORRESPONDING AUTHOR: Y. ZHAO (e-mail: zhao-yue@szu.edu.cn)

This work was supported by the Key Research and Development Project of Guangdong Province under Grant 2020B0101080001.

ABSTRACT In this paper, a dual-band dual-polarized antenna with isolation enhancement is designed. The proposed antenna operates in the frequency range of 3.4–3.6 GHz and 4.8-5 GHz, where the center frequency of the high band (HB) is 1.4 times that of the low band (LB). Two radiating patches are placed in different layers to create the two distinct resonances and the bottom patch which is shorted to the ground by four metal posts acts as the ground for the top patch antenna. A metal wall is introduced between LB feeding probes to enhance the polarization isolation to more than 25 dB. Complementary split-ring resonator (CSRR) structures are etched on the feedlines to improve the cross-band isolation to over 25 dB. Based on this antenna element, a 1×4-element linear array is constructed with SRR-loaded baffles positioned between adjacent elements to suppress the mutual coupling. Measured results show that the proposed antenna and its array are good candidates for 5G base station applications.

INDEX TERMS Antenna array mutual coupling, antenna arrays, dual-polarized antennas.

I. INTRODUCTION

WITH the advancement in modern wireless communication technologies, systems are required to support an expanding number of frequency bands. Antennas that support more than one band are attractive due to their compact size and possibly low cost. In addition, base station antennas are usually designed to be dual-polarized to reduce multipath fading and increase channel capacity [1], [2], [3], [4]. Therefore, dual-band and dual-polarized (DBDP) antennas are becoming increasingly popular in base station applications.

Various dual-band antennas have been proposed in the literature [5], [6], [7], [8], [9], [10], [11], [12], [13], [14], [15], [16], [17], [18] which can be divided into two categories, using a single radiator and using distinct radiators. Exciting different modes of a single radiator can generate dual bands as shown in [5] where slots are cut on a single patch to realize dual bands from a single port, however, the down-tilt angle of the two bands cannot be controlled independently. Designs in [6], [7], [8], [9], [10], [11], [12], [13], [14], [15], [16], [17], [18] use separate radiators. Placing high-band (HB) radiators next to [6] or around [7] low-band (LB) radiators requires a large footprint and is therefore not suitable for compact designs. Placing the HB radiators below the LB radiators saves space, but the consequent disadvantage is the severe radiation blocking by the LB radiator. To address this problem, LB radiators are designed as frequency-selective surfaces that allow HB waves to pass through [10], [11], [12] and an additional layer working as a partially reflective surface is adopted to restore the HB radiation patterns [13]. Another arrangement scheme is placing the HB antennas above the LB, which has a relatively high profile but less pattern distortion. In [14], [15], frequency selective surfaces (FSSs) are used as HB grounds while allowing LB waves to pass through. In [16], [17], a straightforward structure is created by stacking the HB and LB patches vertically and using the LB patches as the HB ground.

Isolation, including cross-band isolation, in-band isolation between ports with different polarizations and in-band isolation between elements in arrays, is one key parameter for the DBDP antennas, especially when the HB and LB antennas are packed in a crowded space and for the application of massive multiple-in-multiple-output (MIMO) systems [19] where tens or hundreds of units are in close

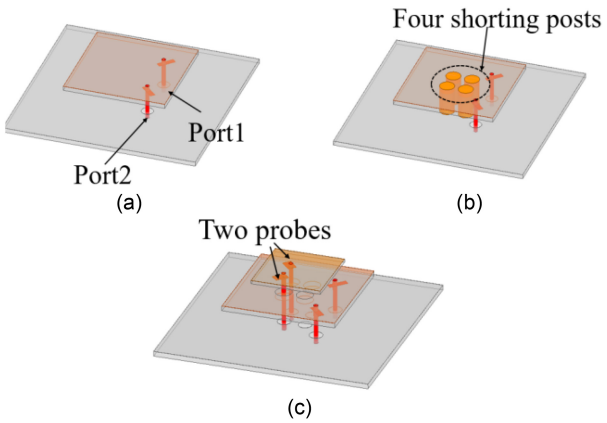

FIGURE 1. Evolution procedure of the proposed antenna: (a) dual-polarized patch antenna, (b) antenna with shorting posts, and (c) dual-band dual-polarized antenna.

proximity. Many efforts have been made to suppress those unwanted couplings. Creating an out-of-phase coupling by ground metal walls [20], decoupling surfaces [21], and neutralization lines [22] to cancel out the original one is one popular way to increase the in-band isolation. Baffles [23] are also often employed to improve the in-band isolation between adjacent elements. To improve the cross-band isolation, filtering structures integrated into the radiators or the feedlines are used. A parasitic loop is loaded under the HB radiator to create a radiation null in the LB and thus improves the cross-band isolation [10]. With stubs loaded to the feedlines, virtual series opens or parallel shorts can be realized and therefore prevent unwanted signals [7], [9], [10], [18].

In this paper, a compact dual-band dual-polarized patch antenna with isolation enhancement is presented for sub-6 GHz base stations. The two operating bands are close to each other with a frequency ratio of 1.4. Complementary split-ring resonator (CSRR) filtering structures and metal walls are introduced to improve the cross-band isolation and polarization isolation of the proposed patch antenna. A 1×4 array is designed for MIMO applications with SRR-loaded baffles positioned between adjacent elements to suppress the mutual coupling among antenna units. Good performance is achieved making the proposed antenna a potential candidate for 5G sub-6 GHz base station systems.

II. ANTENNA DESIGN AND OPERATION PRINCIPLE

A. ANTENNA GEOMETRY

Fig. 1 shows the evolution procedure of the proposed dual-band patch antenna, which is initiated from a conventional dual-polarized patch antenna. As shown in Fig. 1(a), when the patch antenna is fed at Port1 or Port2, dominant mode TM10 or TM01 is excited for radiation. According to the well-known cavity model theory [24], the electric field intensity of the fundamental patch antenna mode is vanishingly small in the center, which indicates that the center of the radiating patch can be shorted to the ground while maintaining the fundamental mode, as shown in Fig. 1(b) where the four shorting posts are symmetrically located in the center.

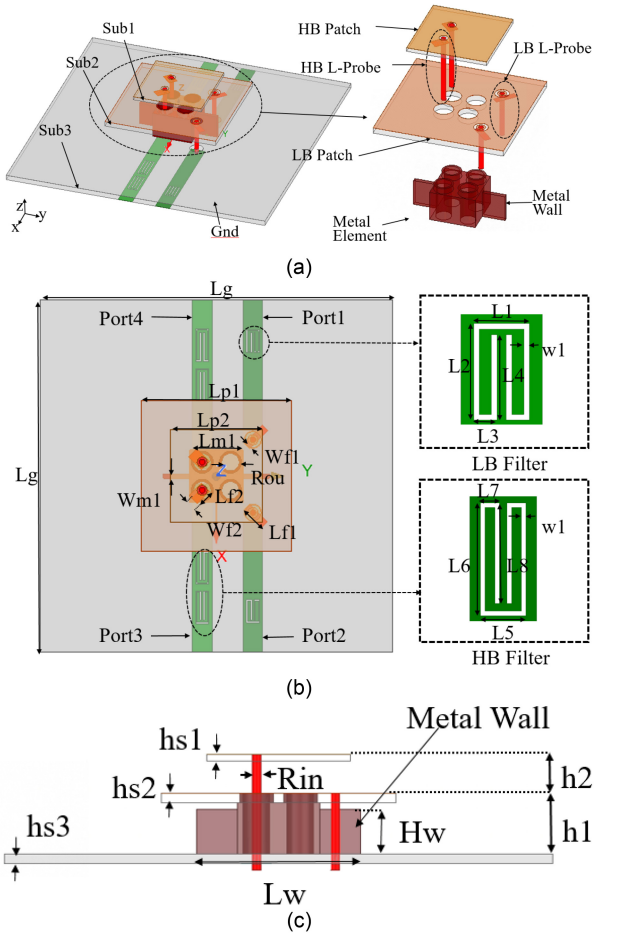

FIGURE 2. Configuration of the proposed antenna unit: (a) overall view, (b) top view, and (c) side view.

In order to realize the dual bands, as depicted in Fig. 1(c), a smaller patch is introduced above the initial patch and the four shorting posts are designed as hollow cylinders. The small patch is designed to resonate in the HB and utilizes the bottom patch as the HB ground. The HB feed probes are inserted into the hollow cylinders to form coaxial cables that transfer energy to excite the HB patch antenna. In addition, the antenna is designed with dual slant ±45° polarizations to meet the requirement of the base station antennas.

Fig. 2 shows the configuration of the proposed antenna unit which is composed of three layers of substrates, a metal element, and four L-probe feeds. The substrates are Wangling F4BM220 laminates with a permittivity of 2.2, and a loss tangent of 0.002. The HB radiating patch and the horizontal part of the HB L-probe feeds are printed on the top and bottom surfaces of Sub1, and the LB radiating patch and the horizontal part of the LB L-probe feeds are on the top and bottom surfaces of Sub2. The top surface of Sub3 serves as the antenna ground and the bottom surface is printed with four microstrip lines connecting the four L-probes to four ports, where Port1 and Port2 are the LB ports, and Port3 and Port4 are the HB ports. It is noted that the microstrip lines

TABLE 1. Parameters of the proposed antenna (unit: *mm*).

Parameters	Lg	Lp1	Lp2	Lm1	Wm1	Lf1	Wf1
value	80	34.2	21	11	1	5.8	1.7
Parameters	Lf2	Wf2	Rou	Rin	h1	h2	L1
value	4	2.6	4	1.3	7.5	6	3
parameters	L2	L3	L4	L5	L6	L7	L8
value	5.2	1.25	4.6	3	7.4	1.25	6.6
Parameters	W1	hs1	hs2	hs3	Lw	Hw	
value	0.3	1	1.5	1.5	24	5	

are etched with several CSRRs which helps in improving the cross-band isolation between the HB and LB ports, as will be discussed later. The metal element is composed of four metal hollow posts and a sticking-out metal wall, which are fabricated by CNC machining and are built as a single structure for the convenience of processing. The metal wall is located between the two LB L-probes to enhance the LB isolation between Port1 and Port2. The dimensions of the antenna element are displayed in Table 1.

B. MECHANISM OF ISOLATION ENHANCEMENT

In this part, two methodologies adopted to improve the isolation of the proposed antenna unit are discussed.

In order to improve the polarization isolation between the two LB ports (Port1 and Port2), a grounded metal wall as shown in Fig. 2 is placed between the two LB L-probes. When there is no metal wall, the isolation between Port1 and Port2 is about 20 dB. As has been discussed in [20] that the poor isolation between the two ports is mainly due to the strong coupling between the vertical part of the probes, hence a metallic wall with a length of Lw1 is placed between the two probes to improve the isolation as shown in the subgraph of Fig. 3(a) where the HB components are made invisible. As Lw1 increases, the isolation significantly improves and has its best performance within the band from 3.4 to 3.6 GHz when Lw1 is 12 mm. In order to further improve the isolation, the metal wall is extended with a length of Lw2 in the opposite direction as depicted in the subgraph of Fig. 3(b). It can be observed that, with the increase of Lw2, the valley at 3.5 GHz deepens while the performance below 3.45 GHz degrades, hence Lw2 is chosen to be 12 mm. With the introduced metal wall, the isolation is improved to more than 40 dB and is better than 25 dB within the desired band.

To improve the cross-band isolation between the LB ports and HB ports, CSRRs [25] that function as half-wavelength resonators are employed as shown in Fig. 2(b). The HB CSRRs are etched on the LB microstrip lines, while the LB CSRRs are etched on the HB microstrip lines. It is observed that the LB CSRRs are larger compared with the HB CSRRs because the former ones exhibit a lower resonant frequency in order to filter out the LB signals. Fig. 4(a) shows the comparison of the surface current distribution with and without the filtering structure. It can be observed that when Port1 (LB port) is excited and there are no CSRRs on the HB microstrip lines, a small portion of current flows to the HB microstrip lines. In particular, the microstrip line of Port3,

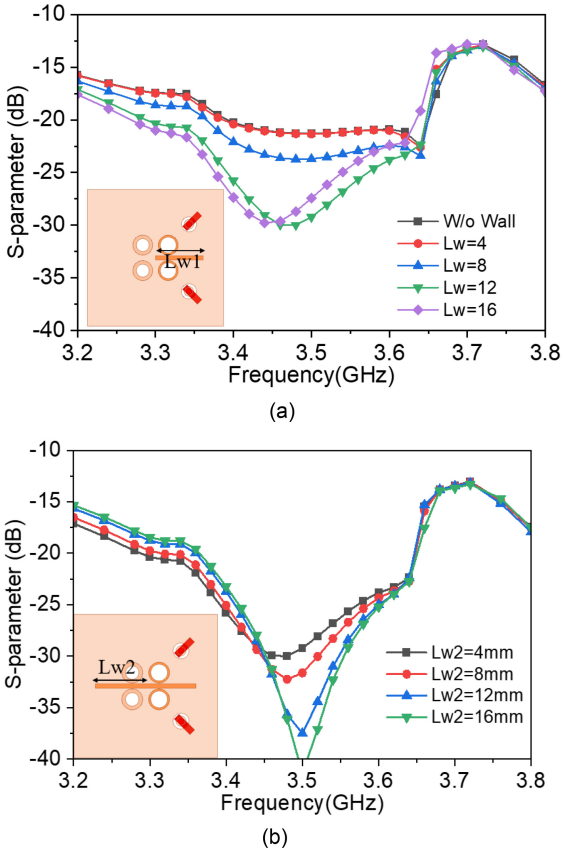

FIGURE 3. Effect of the metal wall on |S21|: (a) varying Lw1, and (b) varying Lw2.

which has the same polarization as Port1, experiences a significant current flow. When the CSRRs are added to the HB microstrip lines, a resonance is observed at the CSRRs and very faint fields can pass through the CSRRs and flow to Port3. As a result, the introduction of the CSRRs to the microstrip lines can enhance the isolation between different bands. Similarly, etching the HB CSRRs on the LB microstrip lines can also restrict the HB signals from entering the LB ports. In this way, high cross-band isolation is achieved in both the HB and LB. Fig. 4(b) gives the isolation between the LB and HB ports (S13) with and without the CSRRs. When there is no CSRR, the cross-band isolation is merely 13 dB in the LB and 18 dB in the HB. With one LB CSRR and one HB CSRR added, the cross-band isolation within the band is improved to more than 25 dB in the HB while it is merely 16 dB in the LB. As a result, one more LB CSRR is introduced and the LB cross-band isolation is improved to above 30 dB. Fig. 4(c) shows the influence of CSRRs on the reflection coefficient. It can be observed that adding CSRRs to the microstrip lines has little influence on matching. As the size of the CSRR is critical to the resonance frequency, as shown in Fig. 5, the length L2 is varied to demonstrate the influence of the size of CSRR on the cross-band isolation. As L2 decreases from 4.9 to 5.3 mm, the central frequency of the operating band shifts from 5.1 to 4.75 GHz. In the proposed design, L2 is set to

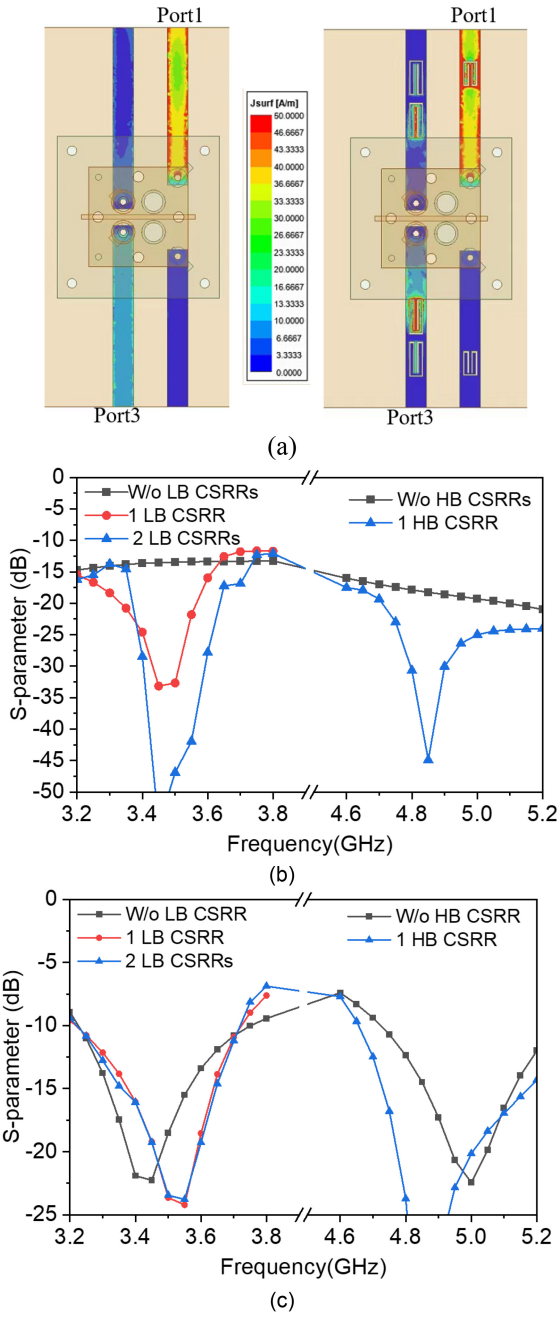

FIGURE 4. Effect of the CSRRs: (a) current distribution on the feedlines, (b) isolation and (c) reflection coefficient.

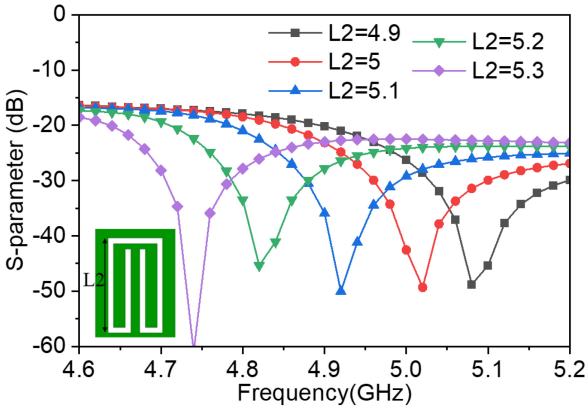

FIGURE 5. HB cross-isolation for different size of CSRR.

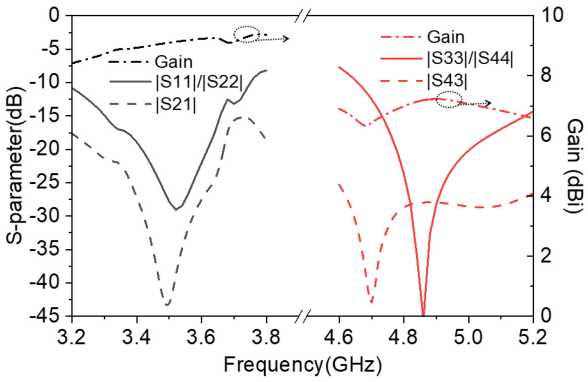

FIGURE 6. S-parameters and gains in the LB and HB.

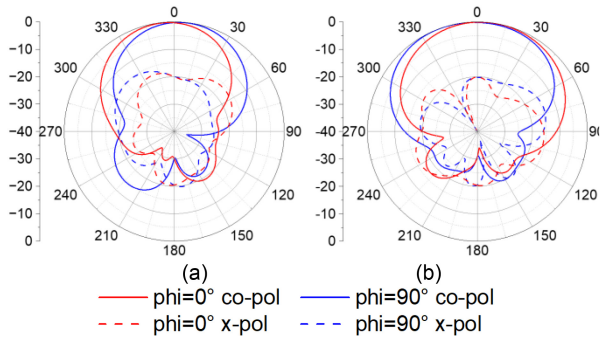

FIGURE 7. Simulated radiation patterns of the proposed antenna at: (a) 3.5 GHz, and (b) 4.9 GHz.

be 5.2 mm to fulfill the requirement of less than 25 dB of the cross-band isolation from 4.8 to 5 GHz.

C. ANTENNA PERFORMANCE

Fig. 6 shows the simulated S-parameters and gains in the LB and HB. The reflection coefficients are lower than −15 dB in the LB from 3.4 to 3.6 GHz and in the HB from 4.8 to 5 GHz. Benefiting from the filtering structure, both the in-band and cross-band isolations (|S13|, |S14|, |S23|, |S24|) are better than 25 dB in the LB and HB. The simulated gains are between 8.9 and 9.3 dBi in the LB and between 7 and 7.2 dBi in the HB. Fig. 7 displays the simulated normalized radiation pattern at 3.5 and 4.9 GHz. The simulated half-power beamwidth (HPBW) is 57° in both the horizontal and vertical planes at 3.5 GHz. At 4.9 GHz, the HPBW is 87° in the horizontal plane and 96° in the vertical plane. The simulated cross-polarizations are less than −15 dB.

III. ANTENNA ARRAY

A 1 × 4 linear array is designed and manufactured to meet the demand for MIMO applications, as shown in Fig. 8. The distance between the centers of the element is 44 mm, which is 0.5 λ_0 at 3.5 GHz and 0.7 λ_0 at 4.9 GHz. Due to

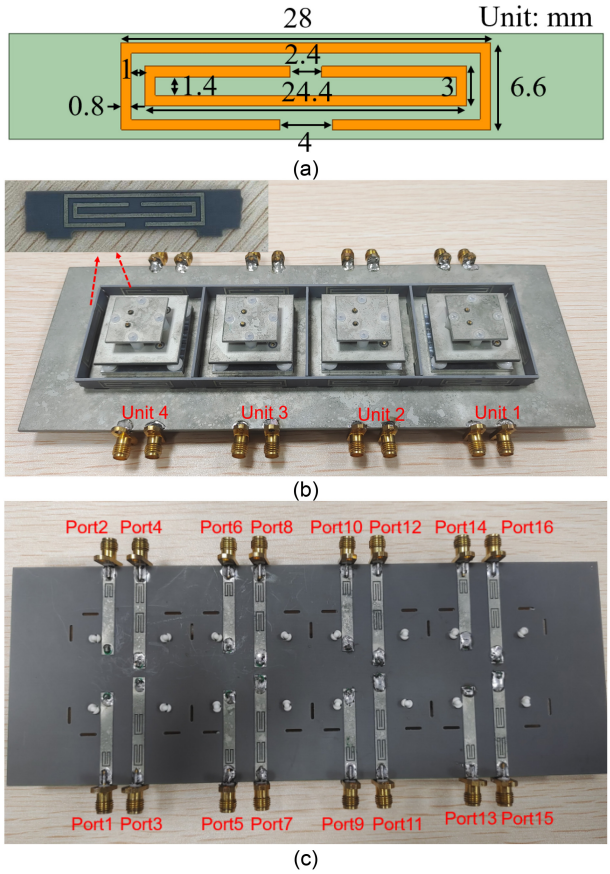

FIGURE 8. Fabricated prototype of the antenna array: (a) baffle, (b) top view, and (c) bottom view.

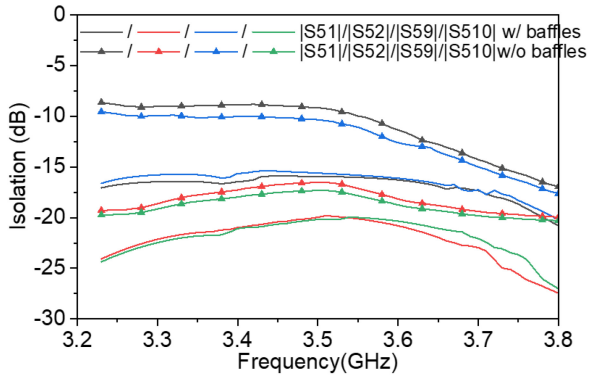

FIGURE 9. Port isolation between adjacent antenna units with and without the SRR baffles.

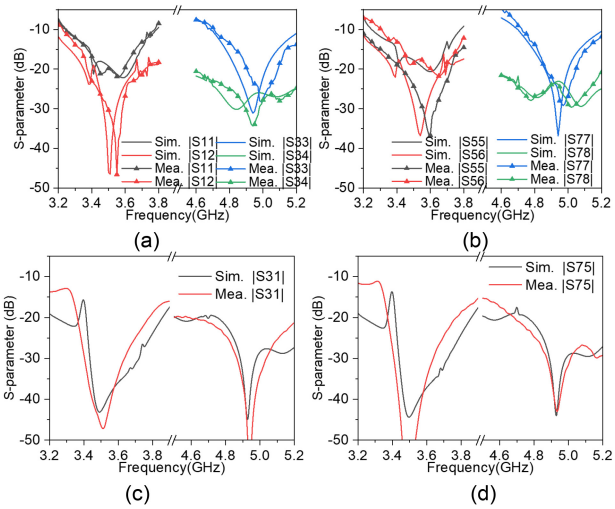

FIGURE 10. Simulated and measured results of the S-parameter for Unit1 and Unit2: (a) reflection coefficient and isolation of Unit1, (b) reflection coefficient and isolation of Unit2, (c) isolation between LB and HB of Unit1, and (d) isolation between LB and HB of Unit2.

the small distance between adjacent antennas, especially at 3.5 GHz, the port isolation between the adjacent antennas is unsatisfactory. To address this problem, baffles loaded by SRRs [23] are added. It has been demonstrated that the SRR works as a band-stop filter whose operating frequency is determined by the equivalent inductance and capacitance which can be adjusted by varying the length, width, and gap of the SRR [23], [26]. It is well known that the patch antenna can be treated as a cavity bonded by two electric walls on the top and bottom and four magnetic walls on the rest [24]. Transverse magnetic fields and longitudinal electric fields along the radiating edges are observed. In the proposed design, the element is 45° slant-polarized and the baffles are along the x and y axes so that the SRRs can be magnetically excited, reducing the coupling between adjacent elements. Fig. 9 shows the isolation between the adjacent antenna units with and without the baffles. The port isolation between adjacent antenna units is merely −9 dB without the SRRs. When the SRRs are introduced, the isolation is increased to more than 16 dB. Adding SRR baffles can significantly improve the isolation between adjacent elements.

Due to the symmetrical structure of the antenna array, only the results of Unit1 and Unit2 are given. Fig. 10 shows the measured and simulated results of the S parameters. The measured and simulated results are in good agreement. Some of the results are biased because of fabrication errors. The measured |S11| and |S55| are lower than −15 dB from 3.4 to 3.6 GHz for the LB, and |S33| and |S77| are lower than −15 dB from 4.8 to 5.1 GHz for the HB. High polarization isolation (>25 dB) is achieved for both the LB and HB. Benefiting from the introduction of the SRRs to the microstrip lines, the cross-band isolation between the LB and HB ports is higher than 30 dB in the LB and higher than 25 dB in the HB. Fig. 11 shows the isolation between adjacent antenna units, the most serious mutual coupling is seen between the two ports with the same polarization (Port1 and Port5, Port5 and Port9). In the LB, |S51| and |S59| are better than 16 dB and the isolation between ports with orthogonal polarizations is higher than 20 dB. In the HB, because of the large spacing compared with the free space wavelength, the isolation between adjacent antenna units is greater than 22 dB.

As the array is proposed for the MIMO application, the envelope correlation coefficient (ECC) performance is

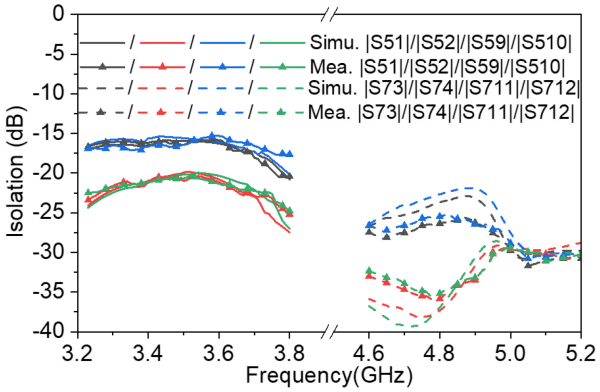

FIGURE 11. Isolation between adjacent antenna units.

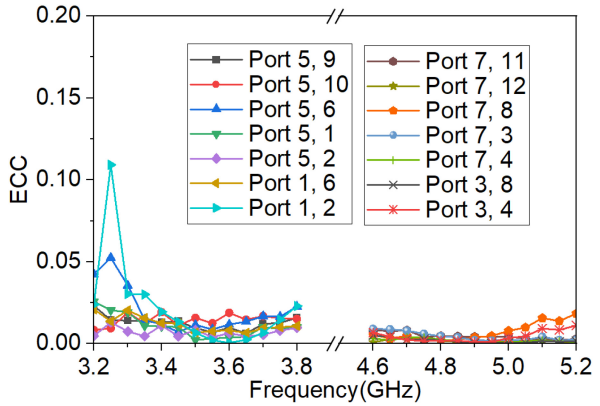

FIGURE 12. Measured ECC of the proposed MIMO array.

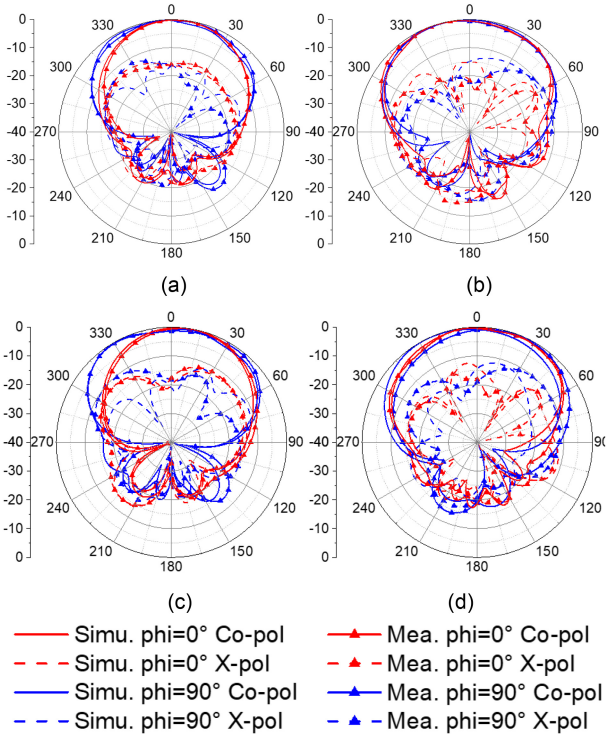

FIGURE 13. Simulated and measured radiation patterns: (a) Unit1 at 3.5 GHz, (b) Unit1 at 4.9 GHz, (c) Unit2 at 3.5 GHz, and (d) Unit2 at 4.9 GHz.

TABLE 2. Comparison with state-of-the-art dual-band dual-polarized antennas.

Ref.	Ant. type	Bands (GHz)	Freq. ratio	Total height	Iso*	Array		
						Ele. No.	Ele. Distance	Ele. iso.**
[9]	Dipole Dipole	1.7-2.7 4.2-5	2.1	$0.27\lambda_{lc}$ $0.58\lambda_{hc}$	>28	/	/	/
[12]	Patch Patch	2.3–2.7 3.3–3.8	1.42	$0.21\lambda_{lc}$ $0.3\lambda_{hc}$	/	/	/	/
[7]	Dipole Dipole	2.5–2.7 3.3-3.6	1.33	$0.21\lambda_{lc}$ $0.28\lambda_{hc}$	>25	1×4 1×4	$0.65\lambda_{lc}$ $0.86\lambda_{hc}$	/
[27]	Dipole Dipole	1.8–2.7 3.3–3.8	1.6	$0.24\lambda_{lc}$ $0.38\lambda_{hc}$	>20 >20	1×2 2×4	$0.94\lambda_{lc}$ $0.5\lambda_{hc}\times$ $0.74\lambda_{hc}$	>20; >20
[28]	Dipole Patch	0.79–0.86 0.88-0.96	1.14	$0.23\lambda_{lc}$ $0.27\lambda_{hc}$	>17	1× 9	$0.77\lambda_{lc}$ $0.86\lambda_{hc}$	/
This	Patch Patch	3.4-3.6 4.8-5	1.4	$0.17\lambda_{lc}$ $0.24\lambda_{hc}$	>30 >25	1×4 1×4	$0.51\lambda_{lc}$ $0.72\lambda_{hc}$	>16; >22

λ_{lc} is the wavelength at the LB central frequency;
λ_{hc} is the wavelength at the HB central frequency;
* Cross-band isolation; ** isolation between adjacent elements.

investigated and the results are plotted in Fig. 12. It can be observed that all the ECCs are less than 0.025 across the operating bands, far less than the general criteria of ECC < 0.3.

Fig. 13 depicts the simulated and measured radiation patterns of Unit1 and Unit2 in the array. The measured HPBWs of Unit1 are 58° at 3.5 GHz and 96° at 4.9 GHz in the horizontal plane, and in the vertical plane, the HPBWs are 88° and 94° respectively. Unit 2 shows a similar performance with the measured HPBWs of 66° at 3.5 GHz and 92° at 4.9 GHz in the horizontal plane and 100° and 92° respectively in the vertical plane. The measurement results demonstrate that in the operating range of 3.4 to 3.6 GHz, Unit1 and Unit2 achieve maximum gains of 6.8 dBi and 7.4 dBi respectively, and in the HB from 4.8 to 5 GHz, the two units obtain maximum gains of 6.8 dBi and 6.9 dBi respectively.

Table 2 lists the key characteristic of some state-of-the-art dual-band dual-polarized antennas and the proposed one for comparison. It can be observed that unlike the designs in [7], [9], [27] and [28], which utilize dipoles or dipole combined with patch antennas to realize the dual-band performance, the proposed one adopts only patch antennas, and since the patch antennas are typically thinner than the dipoles, the proposed one has a lower profile. In contrast to the designs presented in [27] and [28], which exhibit cross-band isolation levels of 20 dB and 17 dB, respectively, the suggested design attains superior cross-band isolation, surpassing 25 dB in the LB and 30 dB in the HB. Further enhancement of isolation is feasible by incorporating more CSRRs onto the feedlines. Unlike the array configurations in [7] and [28], the proposed design features reduced inter-element spacing, enabling wider beam steering angles. In addition, the proposed antenna has an advantage of a simple structure, and can be extended to support more bands by simply stacking additional patches in ascending size order

from bottom to top, grounding the central of the patches to allow feeds to pass through and integrating CSRRs on the feedlines to guarantee cross-band isolation.

IV. CONCLUSION

In this paper, a dual-band dual-polarized base station antenna with isolation enhancement is proposed. The dual-band dual-polarized antenna is realized by introducing shorting post to form a stacked structure. The metal wall is designed to improve the polarization isolation between the LB ports to more than 25 dB, and the cross-band isolation is enhanced to over 25 dB by the CSRRs. A 1×4 linear array with SRR-loaded baffles is designed, manufactured and tested. The measured results demonstrate that 5G operating bands of 3.4–3.6 and 4.8-5.0 GHz are fully supported with good radiation patterns, small reflection coefficients and high isolation. The proposed antenna can be a solution for 5G MIMO base station systems.

REFERENCES

[1] M. Ciydem and E. A. Miran, "Dual-polarization wideband sub-6 GHz suspended patch antenna for 5G base station," *IEEE Antennas Wireless Propag. Lett.*, vol. 19, no. 7, pp. 1142–1146, Jul. 2020.

[2] H. Huang, Y. Liu, and S. Gong, "A broadband dual-polarized base station antenna with sturdy construction," *IEEE Antennas Wireless Propag. Lett.*, vol. 16, pp. 665–668, 2017.

[3] Y. Cui, R. Li, and H. Fu, "A broadband dual-polarized planar antenna for 2G/3G/LTE base stations," *IEEE Trans. Antennas Propag.*, vol. 62, no. 9, pp. 4836–4840, Sep. 2014.

[4] H. Wong, K.-L. Lau, and K.-M. Luk, "Design of dual-polarized L-probe patch antenna arrays with high isolation," *IEEE Trans. Antennas Propag.*, vol. 52, no. 1, pp. 45–52, Jan. 2004.

[5] Y. Li, Z. Zhao, Z. Tang, and Y. Yin, "Differentially fed, dual-band dual-polarized filtering antenna with high selectivity for 5G Sub-6 GHz base station applications," *IEEE Trans. Antennas Propag.*, vol. 68, no. 4, pp. 3231–3236, Apr. 2020.

[6] Y. Zhang, X. Y. Zhang, L.-H. Ye, and Y.-M. Pan, "Dual-band base station array using filtering antenna elements for mutual coupling suppression," *IEEE Trans. Antennas Propag.*, vol. 64, no. 8, pp. 3423–3430, Aug. 2016.

[7] Y. Liu, S. Wang, N. Li, J.-B. Wang, and J. Zhao, "A compact dual-band dual-polarized antenna with filtering structures for sub-6 GHz base station applications," *IEEE Antennas Wireless Propag. Lett.*, vol. 17, no. 10, pp. 1764–1768, Oct. 2018.

[8] L. Ye, Y. Cao, and X. Z. Xiuyin, "Multibeam antenna based on butler matrix for 3G/LTE/5G/B5G base station applications," *ZTE Commun.*, vol. 18, no. 3, pp. 12–19, 2020.

[9] Y. Zhang and Y. Zhang, "Dual-band dual-polarized antenna using a simple radiation restoration and decoupling structure," *IEEE Antennas Wireless Propag. Lett.*, vol. 22, no. 4, pp. 709–713, Apr. 2023.

[10] S. J. Yang, R. Ma, and X. Y. Zhang, "Self-decoupled dual-band dual-polarized aperture-shared antenna array," *IEEE Trans. Antennas Propag.*, vol. 70, no. 6, pp. 4890–4895, Jun. 2022.

[11] G.-N. Zhou, B.-H. Sun, Q.-Y. Liang, S.-T. Wu, Y.-H. Yang, and Y.-M. Cai, "Triband dual-polarized shared-aperture antenna for 2G/3G/4G/5G base station applications," *IEEE Trans. Antennas Propag.*, vol. 69, no. 1, pp. 97–108, Jan. 2021.

[12] S. J. Yang and X. Y. Zhang, "Frequency selective surface-based dual-band dual-polarized high-gain antenna," *IEEE Trans. Antennas Propag.*, vol. 70, no. 3, pp. 1663–1671, Mar. 2022.

[13] Y. Qin, R. Li, Q. Xue, X. Zhang, and Y. Cui, "Aperture-shared dual-band antennas with partially reflecting surfaces for base-station applications," *IEEE Trans. Antennas Propag.*, vol. 70, no. 5, pp. 3195–3207, May 2022.

[14] Y. Zhu, Y. Chen, and S. Yang, "Integration of 5G rectangular MIMO antenna array and GSM antenna for dual-band base station applications," *IEEE Access*, vol. 8, pp. 63175–63187, 2020.

[15] Y. Zhu, Y. Chen, and S. Yang, "Decoupling and low-profile design of dual-band dual-polarized base station antennas using frequency-selective surface," *IEEE Trans. Antennas Propag.*, vol. 67, no. 8, pp. 5272–5281, Aug. 2019.

[16] P. Li, K. M. Luk, and K. L. Lau, "A dual-feed dual-band L-probe patch antenna," *IEEE Trans. Antennas Propag.*, vol. 53, no. 7, pp. 2321–2323, Jul. 2005.

[17] X. Yang et al., "An integrated tri-band antenna system with large frequency ratio for WLAN and WiGig applications," *IEEE Trans. Ind. Electron.*, vol. 68, no. 5, pp. 4529–4540, May 2021.

[18] S. J. Yang, W. Duan, Y. Y. Liu, H. Ye, H. Yang, and X. Y. Zhang, "Compact dual-band base-station antenna using filtering elements," *IEEE Trans. Antennas Propag.*, vol. 70, no. 8, pp. 7106–7111, Aug. 2022.

[19] J. Zhang, C. Wang, Z. Wu, and W. Zhang, "A survey of massive MIMO channel measurements and models," *ZTE Commun.*, vol. 51, no. 1, pp. 14–22, 2017.

[20] K. M. Luk, K. L. Lau, and T. Po, "Isolation enhancement technique for dual polarized probe fed patch antenna," U.S. Patent 7 994 985 B2, Aug. 9, 2011.

[21] J. Yin, Y. Jia, S. Yang, and H. Zhai, "Design of a composite decoupling structure for dual-band dual-polarized base station array," *IEEE Antennas Wireless Propag. Lett.*, vol. 21, no. 7, pp. 1408–1412, Jul. 2022.

[22] Z. Wang and Q. Wu, "A novel decoupling feeding network for circularly polarized patch arrays using orthogonal mode decomposition," *IEEE Trans. Antennas Propag.*, vol. 71, no. 2, pp. 1448–1457, Feb. 2023.

[23] M. Li, X. Chen, A. Zhang, W. Fan, and A. A. Kishk, "Split-ring resonator-loaded baffles for decoupling of dual-polarized base station array," *IEEE Antennas Wireless Propag. Lett.*, vol. 19, no. 10, pp. 1828–1832, Oct. 2020.

[24] C. A. Balanis, *Antenna Theory: Analysis and Design*, 3rd ed. Hoboken, NJ, USA: Wiley, 2005.

[25] Y. Dan Dong, T. Yang, and T. Itoh, "Substrate integrated waveguide loaded by complementary split-ring resonators and its applications to miniaturized waveguide filters," *IEEE Trans. Microw. Theory Techn.*, vol. 57, no. 9, pp. 2211–2223, Sep. 2009.

[26] J. D. Baena et al., "Equivalent-circuit models for split-ring resonators and complementary split-ring resonators coupled to planar transmission lines," *IEEE Trans. Microw. Theory Techn.*, vol. 53, no. 4, pp. 1451–1461, Apr. 2005.

[27] D. He, Q. Yu, Y. Chen, and S. Yang, "Dual-band shared-aperture base station antenna array with electromagnetic transparent antenna elements," *IEEE Trans. Antennas Propag.*, vol. 69, no. 9, pp. 5596–5606, Sep. 2021.

[28] W. Duan, Y. F. Cao, Y.-M. Pan, Z. X. Chen, and X. Y. Zhang, "Compact dual-band dual-polarized base-station antenna array with a small frequency ratio using filtering elements," *IEEE Access*, vol. 7, pp. 127800–127808, 2019.